Simulation of dynamical interaction between dislocations and dipolar loops

Vojtěch Minárik,[1,a)] Michal Beneš,[1,a)] and Jan Kratochvíl[2,b)]

[1]*Department of Mathematics, Faculty of Nuclear Sciences and Physical Engineering, Czech Technical University in Prague, Trojanova 13, 120 00 Prague, Czech Republic*
[2]*Department of Physics, Faculty of Civil Engineering, Czech Technical University in Prague, Thákurova 7, 166 29 Prague, Czech Republic*

The article describes a model of interaction dynamics between a dislocation and dipolar dislocation loops. The interaction is essential for dipolar dislocation structure formation in early stages of a hardening process. For the description of the dislocation curve a direct parametric approach is employed whereas the loops are treated as rigid objects. The model equations are solved approximately by means of the finite-volume method. Physically interesting phenomena can be captured by the model provided the simulation covers long time periods. The strong interaction between the dislocation and the loops causes growing nonuniformity of distribution of discrete nodes along the dislocation curve. This effect is balanced by two proposed types of tangential redistribution of the discrete nodes. The redistribution is tested in simulations of loop clustering. © *2010 American Institute of Physics*. [doi:10.1063/1.3340518]

I. INTRODUCTION

In crystalline solids plastic deformation is carried by dislocations which are line defects of the crystal lattice. Theoretical description of dislocations is provided in classical literature such as Ref. 1 or 2. Along the dislocation curve the regularity of the crystallographic arrangement of atoms is disturbed. The dislocation can be represented by a curve closed inside the crystal or by a curve ending on surface of the crystal. At low homologous temperatures the dislocations can move only along crystallographic planes with the highest density of atoms (slip planes). The motion results in mutual slipping of neighboring parts of the crystal along the slip planes. The slip displacement carried by a single dislocation, called Burgers vector, is equal to one of the vectors connecting the neighboring atoms.

A field induced by displacement of atoms from their regular crystallographic positions in the vicinity of a dislocation curve can be treated as the elastic stress and the strain fields. On the other hand, a stress field exerts a force on a dislocation. The combination of these two effects causes the elastic interaction among dislocations.

One of the most distinguished features of plastic deformation at the microscale is a great overproduction of dislocations during a deformation process. Only a small fraction of generated dislocations is needed to carry plastic deformation, the rest is stored in the crystal. The deformed crystals supersaturated with dislocations tend to decrease the internal energy by mutual screening of their elastic fields. If dislocations possess a sufficient maneuverability provided by easy cross-slip (solids with wavy slip) the leading mechanism is an individual screening. The dislocations are stored in the form of dipoles which are transformed to prismatic dislocation dipolar loops of the prevailing edge character or such

loops are directly formed. The loops are swept into clusters (tangles, veins, dipolar walls) forming pattern of dipolar dislocation structures (the experimental evidence is summarized in Ref. 3).

The glide dislocations (*dislocation curves*) and the dislocation loops (*dipolar loops*) have much different characteristic length scales and mobile properties (see Refs. 4 and 5) as follows:

- The segments of glide dislocations extend over distances of micrometers, whereas size of the prismatic dipolar loops is of the order of 10 nm.
- Glide dislocations are driven by the shear stress resolved in the slip plane, while loops are drifted by stress gradients and/or swept by the glide dislocations. Prismatic loops can move along the direction parallel to the direction of their Burgers vector only.
- During deformation glide dislocations become curved. Local curvature of the glide dislocations seems to be one of leading factors controlling the pattering (see Refs. 6 and 7). On the other hand, loops can be approximately treated as rigid objects.

A helpful tool for investigation of elementary interaction processes of plastic deformation is the discrete dislocation dynamics. When treating dislocations, direct numerical simulations originally considered long parallel straight dislocation lines. Later, more physical but considerably more complex three-dimensional (3D) situations of plastic deformation processes were investigated. Application of this approach addressed a variety of mesoscale plasticity problems. Details can be found, e.g., in Refs. 8–15.

Methods treating dynamics of curved dislocations can be divided into the following groups. Some methods consider discrete segments of the curve moving over a discrete lattice (see Refs. 8 and 11). Other methods discretize the curve into piecewise linear (see Refs. 14 and 15) or piecewise polynomially representative segments (see Refs. 12 and 13).

a)Authors to whom correspondence should be addressed. Electronic addresses: vojtech.minarik@fjfi.cvut.cz and michal.benes@fjfi.cvut.cz.
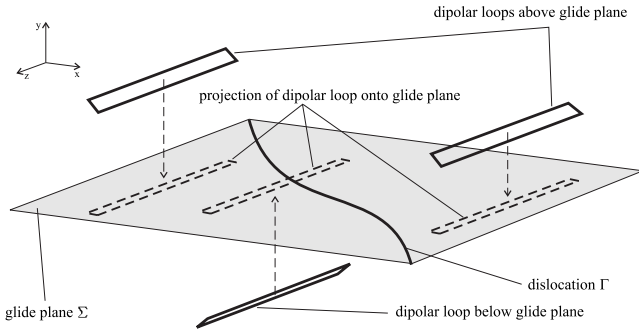b)Electronic mail: kratochvil@fsv.cvut.cz.

FIG. 1. Mutual position of dislocation and dipolar loops with respect to the slip plane.

FIG. 2. Stable configurations V_1 and V_2 of dipolar loops positioned at $[x_0, y_0, z_0]$.

Due to the above mentioned complexity, formation of dislocation structures as a consequence of interactions between dislocations is still an open problem. The aim of this article is to present detailed description of a parametric model treating a single dislocation curve and a finite number of dipolar loops and to present simulation results obtained by this model. As the parametric approach allows a single parameter description of the dislocation curve placed in 3D space, there is a gain in speed of the numerical computation. The numerical model using the *flowing finite volume method* based on the presented mathematical model is described. Difficulties with the numerical stability of the original numerical model (mainly due to the strong force interactions of the dislocation curve with dipolar loops) are discussed and an improved numerical model is proposed which includes *tangential redistribution* of the dislocation-curve discretization.

II. PHYSICAL MODEL

A. Equations of motion

The interaction dynamics between a dislocation curve Γ and dipolar loops $\Lambda_1, \ldots, \Lambda_N$ is studied in the coordinate system shown in Fig. 1. The xz plane represents the dislocation slip plane Σ. The dipolar loops treated as rigid objects[16] are considered in their stable configurations—having long rectangular fixed shapes (see Ref. 14). Therefore, their motion is fully described by motion of their barycenters. They are assumed to have longer edges parallel with the z-axis whereas their shorter edges are parallel with either $[1,1,0]$ or $[1,-1,0]$ vectors. Due to its prismatic character, a dipolar loop can move along the x-axis only, keeping the y and z coordinates constant. The Burgers vector is set as $\vec{b}=[b,0,0]$.

The glide of a planar dislocation curve Γ is governed by the linear viscous law written in the scalar form of the mean curvature flow

$$B v_\Gamma = \varepsilon \kappa_\Gamma + F, \tag{1}$$

relating its normal velocity v_Γ to the curvature κ_Γ and sum F of forces acting on Γ in the normal direction to the dislocation curve. Here, B denotes the drag coefficient and ε stands for the line tension. This evolution law is known from other applications as described in Refs. 17 and 18. As pioneered by Ref. 19, developed by Ref. 20, and under further improve-
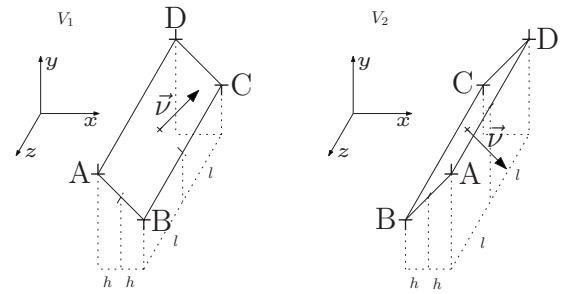
ment of Ref. 12, the law [Eq. (1)] can be treated by the arc-length parametrization. The parametrization is a smooth vector mapping $\vec{X}=\vec{X}(t,s)$ depending on time $t \in (0,T)$ and arc length $s \in (0, L(t))$, where $L(t)$ is the length of the dislocation curve at a given time t. The mapping satisfies the identity $|\partial_s \vec{X}(t,s)| = 1$. Values of $\vec{X}(t,s)$ are in the slip plane Σ. In our setting, this means that the second coordinate of $\vec{X}$ is zero. The motion law [Eq. (1)] is then transformed into the vectorial form as follows:

$$B \partial_t \vec{X} = \varepsilon \partial_{ss}^2 \vec{X} + F \partial_s \vec{X}^\perp,$$

where $\partial_s \vec{X}^\perp$ represents the normal vector to Γ.

The dislocation curve is assumed to be open with fixed ends which provides the boundary conditions for the parametrization

$$\vec{X}(t,0) = \vec{X}_{\text{fixed},0}, \quad \vec{X}(t,L(t)) = \vec{X}_{\text{fixed},L}.$$

A closed dislocation curve (e.g., appearing in the Frank–Read source) can be treated when considering the periodic boundary conditions

$$\vec{X}(t,0) = \vec{X}(t,L(t)).$$

As indicated above, each dipolar loop is assumed to have a rectangular shape and to be in one of two stable 45° orientations either in vacancy (i.e., V_1 and V_2) or interstitial (i.e., I_1 and I_2) configurations. They are denoted according to Fig. 2, where vacancy-loop configurations are shown as an example. We also adopt a simplification assuming that all dipolar loops considered have the same size: their average half-width h, the average half-length l, and the average perimeter P are shown in Fig. 2 and are related as

$$P = 2(2h\sqrt{2} + 2l).$$

The position of a dipolar loop Λ_j, $j=1, \ldots, N$ is given by the coordinates $[x^{(j)}, y^{(j)}, z^{(j)}]$ of its barycenter. According to the previous assumptions, $y^{(j)} = \text{const.} \neq 0$ and $z^{(j)} = \text{const.}$, and $x^{(j)} = x^{(j)}(t)$ satisfies the motion law

$$\frac{dx^{(j)}}{dt} = \frac{1}{BP} F_{x,\text{total}}^{(j)}(\Gamma, x^{(1)}, \ldots, x^{(N)}). \tag{2}$$

The term $F_{x,\text{total}}^{(j)}$ represents the force interaction with other dipolar loops and with the dislocation curve. This interaction is projected to the only possible direction of the loop motion—to the direction of the x-axis.

The interaction dynamics of a dislocation curve Γ and dipolar loops $\Lambda_1, \ldots, \Lambda_N$ is therefore described by the following set of equations endowed by the boundary and initial conditions

$$B\partial_t \vec{X} = \varepsilon \partial_{ss}^2 \vec{X} + F(t,\vec{X},\Lambda_1,\ldots,\Lambda_N)\partial_s \vec{X}^\perp, \tag{3}$$

$$\frac{dx^{(j)}}{dt} = \frac{1}{BP} F_{x,\text{total}}^{(j)}(\Gamma, x^{(1)}, \ldots, x^{(N)}), \tag{4}$$

$$\vec{X}(t,0) = \vec{X}_{\text{fixed},0}, \quad \vec{X}(t,L(t)) = \vec{X}_{\text{fixed},L}, \tag{5}$$

$$\vec{X}(0,s) = \vec{X}_{\text{ini}}(s), \quad x^{(j)}(0) = x_{\text{ini}}^{(j)}, \quad j = 1, \ldots, N. \tag{6}$$

B. Evaluation of interaction terms

Driving force per unit length of the dislocation curve $F = F(t,\vec{X},\Lambda_1,\ldots,\Lambda_N)$ in Eq. (3) is caused by forces exerted to a tested specimen and interaction with dipolar loops; the influence of other dislocations and of lattice friction is not considered

$$F = b\sigma_{\text{local}} + \sum_{j=1}^{N} b\sigma_{xy}^{(j)}.$$

Generally, to determine the local stress σ_{local} at the dislocation curve coming from the forces exerted to the specimen requires a solution of a boundary value problem for a particular experimental setup. Instead of this problem two simplified limit cases are considered: either applied stress or total strain are assumed uniform; the former alternative provides an upper estimate of the local applied stress, while the latter one gives a lower estimate (see Ref. 21). Here the latter technically more challenging alternative, which seems to be closer to the reality, is considered. It means that the total shear strain ε_{tot}, being a sum of the elastic and plastic parts,

$$\varepsilon_{\text{tot}} = \frac{\sigma_{\text{local}}}{\mu} + p, \tag{7}$$

is assumed to be uniform; σ_{local} is the local resolved shear stress and μ is shear modulus (we set $\mu = 80$ GPa). To estimate the plastic strain p the considered dislocation is taken as a representative of glide dislocations in a specimen. The plastic strain carried by a dislocation segment is

$$p(t) = \varrho b \int_0^t \partial_t \vec{X}(\tau) \cdot \partial_s \vec{X}^\perp(\tau) d\tau, \tag{8}$$

where the integral represents the part of the slip plane slipped by a dislocation segment of a unit length; the elementary amount of slip is Burgers vector magnitude b; initially $p(t_0) = 0$. The average scalar density ϱ of the glide dislocations in Eq. (8) represents the number of segments piercing a unit area perpendicular to the segment (we set $\varrho = 10^{13}$ m^{-2}).

In the numerical simulations, we explore the case when the total shear strain $\varepsilon_{\text{tot}} = \varepsilon_{\text{tot}}(t)$ is a periodic function in time with the frequency 1.57 s^{-1} and the amplitude 0.0017. From Eqs. (7) and (8) we get that

$$\sigma_{\text{local}}(t) = \mu \left[\varepsilon_{\text{tot}}(t) - \varrho b \int_0^t \partial_t \vec{X}(\tau) \cdot \partial_s \vec{X}^\perp(\tau) d\tau \right]. \tag{9}$$

Interaction with dipolar loops is given by the xy component of the stress field tensor $\sigma_{xy}^{(j)}$ describing the stress field generated by jth dipolar loop, $j = 1, \ldots, N$. As the loops are considered as rigid objects their stress field can be expressed through analytical formula (see Refs. 4, 14, and 22)

$$\begin{aligned}
\sigma_{xy}(x,y,z) = &-\frac{\mu h b}{2\pi(1-\nu)} \left\{ \left[\frac{l-z}{\varrho_-} + \frac{l+z}{\varrho_+} \right] \right. \\
&\times \left[\frac{x \pm y}{(x^2+y^2)^2} \left(\pm x + y - 8\frac{x^2 y}{x^2+y^2} \right) \right] \\
&+ \left[\frac{l-z}{\varrho_-^3} + \frac{l+z}{\varrho_+^3} \right] \left[\pm \nu + \frac{xy}{(x^2+y^2)^2} \right. \\
&\times (y^2 - 3x^2 \mp 4xy) \right] + \left[\frac{l-z}{\varrho_-^5} + \frac{l+z}{\varrho_+^5} \right] \\
&\left. \times \left[-\frac{3x^2 y(x \pm y)}{x^2+y^2} \right] \right\},
\end{aligned}$$

$$\varrho_- = \sqrt{x^2 + y^2 + (l-z)^2}, \quad \varrho_+ = \sqrt{x^2 + y^2 + (l+z)^2}, \tag{10}$$

The above analytical formula for σ_{xy} is valid under the assumption that the distance $[x,y,z]$ of the dipolar loop from the dislocation curve is large enough compared to the dipolar loop parameter h. The stress field of dipolar loops expressed by the above analytical formula allows to speed up the numerical algorithm for solution of the evolution systems [Eqs. (3)–(6)].

Driving term for a dipolar loop $F_{x,\text{total}}^{(j)}$ in Eq. (4) is given by the following formula:

$$F_{x,\text{total}}^{(j)}(\Gamma, x^{(1)}(t), \cdots, x^{(N)}(t)) = \begin{cases} F_x^{c,(j)} + \sum_{k \neq j} F_x^{j,k} - F_0 & \text{if } F_x^{c,(j)} + \sum_{k \neq j} F_x^{j,k} > F_0 \\ 0 & \text{if } \left| F_x^{c,(j)} + \sum_{k \neq j} F_x^{j,k} \right| < F_0 \\ F_x^{c,(j)} + \sum_{k \neq j} F_x^{j,k} + F_0 & \text{if } F_x^{c,(j)} + \sum_{k \neq j} F_x^{j,k} < -F_0, \end{cases} \tag{11}$$

where the term $F_x^{c,(j)}$ is the x-axis component of the force interaction between the entire dislocation curve Γ and the jth dipolar loop:

$$F_x^{c,(j)} = \int_{\Gamma} \sigma_{xy}(\vec{\varrho}^{(j)})bn_x \mathrm{d}s. \tag{12}$$

In Eq. (12), $\vec{\varrho}^{(j)}$ connects the barycenter of the dipolar loop and a given point on the dislocation curve, and n_x is the x-axis component of the normal vector $\partial_s \vec{X}^{\perp}$ of the dislocation curve. The threshold term F_0 stands for the internal lattice friction, i.e., it describes minimal force needed to bring an arbitrary dipolar loop into motion.

In simulations, the interaction between dipolar loops plays an important role. Hence, it cannot be neglected. The computer simulations[16] and results of Ref. 15 show that the sweeping of two loops by a glide dislocation is much different when the mutual loop interaction is not considered. The term $F_x^{j,k}$, describes mutual interaction between the jth and the kth dipolar loops, $k=1,\ldots,N$, $k \neq j$. This term prevents an arbitrary dipolar loop to move across any other dipolar loop.

The term $F_x^{j,k}$ can be approximately evaluated (see Ref. 23 and references therein) provided the average half-width of a dipolar loop h is small enough compared to the distance between the jth and kth dipolar loops (measured between central points of the rectangles of these two loops). The final formula for $F_x^{j,k}$ has three different forms depending on different combination of the types and configurations of the dipolar loops.

(1) For the combinations V_1-V_2, V_1-I_2, I_1-V_2, I_1-I_2, V_2-V_1, V_2-I_1, I_2-V_1, and I_2-I_1 it holds

$$F_x^{j,k(1)} = -\frac{\mu h^2}{\pi(1-\nu)}b'b''\left\{ \xi_1 \frac{-8x_0^5 + 64x_0^3y_0^2 - 24x_0y_0^4}{(x_0^2+y_0^2)^4} \right.$$
$$+ \xi_{-1}\frac{-4x_0^5 + 32x_0^3y_0^2 - 12x_0y_0^4}{(x_0^2+y_0^2)^3} + \xi_{-3}\left[(1-\nu)x_0 \right.$$
$$+ \frac{-x_0^5 + 8x_0^3y_0^2 - 3x_0y_0^4}{(x_0^2+y_0^2)^2} \right] + \xi_{-5}\left. \left[3x_0^3\frac{-x_0^2+y_0^2}{x_0^2+y_0^2} \right] \right\}. \tag{13}$$

(2) and *(3)* For the combinations V_1-V_1, V_1-I_1, I_1-V_1, and I_1-I_1 (using the upper signs), and for V_2-V_2, V_2-I_2, I_2-V_2, and I_2-I_2 (with the lower signs) the interaction is given by the formula

$$F_x^{j,k(2,3)} = -\frac{\mu h^2}{\pi(1-\nu)}b'b''\left\{ -4\xi_1\frac{x_0^5 \pm 9x_0^4y_0 - 2x_0^3y_0^2 \mp 14x_0^2y_0^3 - 3x_0y_0^4 \pm y_0^5}{(x_0^2+y_0^2)^4} \right.$$
$$+ \xi_{-1}\frac{-2x_0^5 \mp 18x_0^4y_0 + 4x_0^3y_0^2 \pm 28x_0^2y_0^3 + 6x_0y_0^4 \mp 2y_0^5}{(x_0^2+y_0^2)^3} + \xi_{-3}\left[(1+\nu)x_0 + \frac{-x_0^5 \mp 4x_0^4y_0 \pm 8x_0^2y_0^3 + x_0y_0^4}{(x_0^2+y_0^2)^2} \right]$$
$$+ \xi_{-5}\left. \left[-3x_0^3\frac{(x_0 \pm y_0)^2}{x_0^2+y_0^2} \right] \right\}. \tag{14}$$

In the above formulae, we used the following short hand notation:

$$\xi_1 = \rho_0(-2l) - 2\rho_0(0) + \rho_0(2l),$$

$$\xi_{-1} = -\frac{1}{\rho_0(-2l)} + 2\frac{1}{\rho_0(0)} - \frac{1}{\rho_0(2l)},$$

$$\xi_{-3} = -\frac{1}{\rho_0^3(-2l)} + 2\frac{1}{\rho_0^3(0)} - \frac{1}{\rho_0^3(2l)},$$

$$\xi_{-5} = -\frac{1}{\rho_0^5(-2l)} + 2\frac{1}{\rho_0^5(0)} - \frac{1}{\rho_0^5(2l)},$$

$$\rho_0(\omega) = \rho_0(x_0, y_0, z_0, \omega) = \sqrt{x_0^2 + y_0^2 + (z_0 + \omega)^2}.$$

In the formulae (13) and (14), ν is the Poisson ratio ($\nu = 0.31$), b' is the signed magnitude of the Burgers vector of the first dipolar loop and b'' is the signed magnitude of the

Burgers vector of the second dipolar loop. As shown in Ref. 23, the interstitial dipolar loop simply reverses the direction of the interaction force. Then values of b' and b'' are, therefore, set to b for the case of a vacancy dipolar loop, and to $-b$ for an interstitial dipolar loop in Eqs. (13) and (14). The vector $[x_0, y_0, z_0]$ denotes the relative position of the loop barycenters.

The interaction between two dipolar loops has a complex spatial variability. This is demonstrated in Figs. 3–6. Figure 3 shows the interaction force $F_x^{j,k(1)}$ between dipolar loops V_1 and V_2 placed in the same height above the slip plane, i.e., difference in y coordinate vanishes. Forces $F_x^{j,k(2)}$ and $F_x^{j,k(3)}$ have similar graphs when staying in the same height above the slip plane—this can be seen from the formulae: almost all terms having difference in y_0 zero vanish and the rest is up-to-constants similar to $F_x^{j,k(1)}$.

Figures 4–6 present graphs of forces between two dipolar loops of types V_1-V_1 and V_2-V_2 which have the same z-axis coordinate, i.e., difference in z coordinate vanishes. In
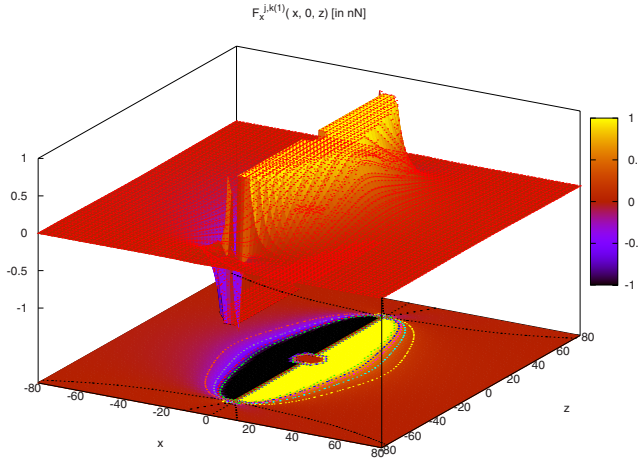
FIG. 3. (Color online) Part of spatial profile of $F_x^{j,k(1)}$ with values between −1 and 1 nN for the interaction between dipolar loops V_1 and V_2 having the same y-axis coordinate (the same distance from the slip plane).

each case, there are five areas where there is attraction between dipolar loops, and five areas where there is repulsion. These areas are of different sizes. Moreover, location of attractive and repulsive areas depends on the combination of dipolar-loop types.

Remark. Note that if we set $x_0 = 0$, there is no force between the dipolar loops, i.e., $F_x^{j,k(1)} = 0$ for any y_0 and z_0. This is not valid for $F_x^{j,k(2)}$ nor for $F_x^{j,k(3)}$.

III. COMPUTATIONAL MODEL

A. Discretization of the evolution problem

The model of interaction dynamics in Eqs. (3)–(6) is approximately treated by means of the numerical scheme based on discretization of the model equations in space by the finite-volume method and subsequently, on discretization of the model equations in time by the higher-order Runge–Kutta scheme.

At a given time moment, the dislocation curve Γ is approximated by a piecewise linear curve with vertices—nodes
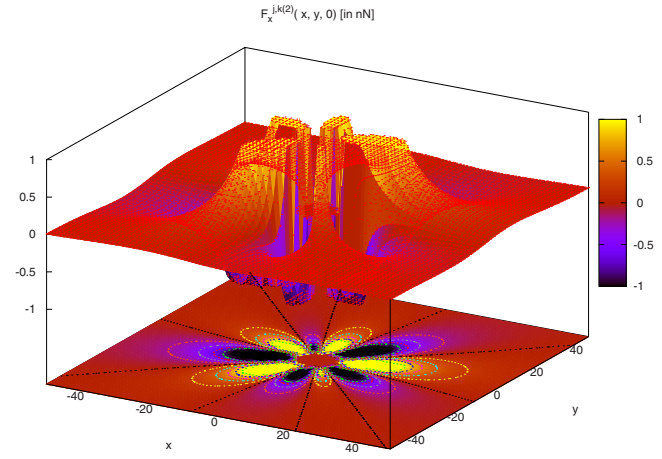
$\vec{X}_i(t)$, $i = 0, \ldots, M$ in the slip plane Σ. The end nodes $\vec{X}_0$ and $\vec{X}_M$ are prescribed by the boundary conditions in Eq. (5)

$$\vec{X}_0 = \vec{X}_{\text{fixed},0}, \quad \vec{X}_M = \vec{X}_{\text{fixed},L},$$

and do not depend on time.

The segments $[\vec{X}_{i-1}, \vec{X}_i]$ are called flowing finite volumes. We also define dual volumes $\mathcal{V}_i = [\vec{X}_{i-(1/2)}, \vec{X}_i] \cup [\vec{X}_i, \vec{X}_{i+(1/2)}]$, $i = 1, .., M-1$, where $\vec{X}_{i-(1/2)} = (\vec{X}_{i-1} + \vec{X}_i)/2$ and $\vec{X}_{i+(1/2)} = (\vec{X}_i + \vec{X}_{i+1})/2$ are the centers of segments $[\vec{X}_{i-1}, \vec{X}_i]$ and $[\vec{X}_i, \vec{X}_{i+1}]$, respectively, (see Fig. 7).

The finite-volume method is based on integrating the evolution [Eq. (3)] over the dual volume $\mathcal{V}_i$. We then obtain

$$\int_{\mathcal{V}_i} B\partial_t \vec{X} ds = \int_{\mathcal{V}_i} \varepsilon \partial_{ss}^2 \vec{X} ds + \int_{\mathcal{V}_i} F\partial_s \vec{X}^\perp ds, \quad (15)$$

from which it follows that

$$B\frac{d_i + d_{i+1}}{2}\frac{d\vec{X}_i}{dt} = \varepsilon[\partial_s \vec{X}]_{\vec{X}_{i-1/2}}^{\vec{X}_{i+1/2}} + F_i[\vec{X}^\perp]_{\vec{X}_{i-1/2}}^{\vec{X}_{i+1/2}}, \quad (16)$$
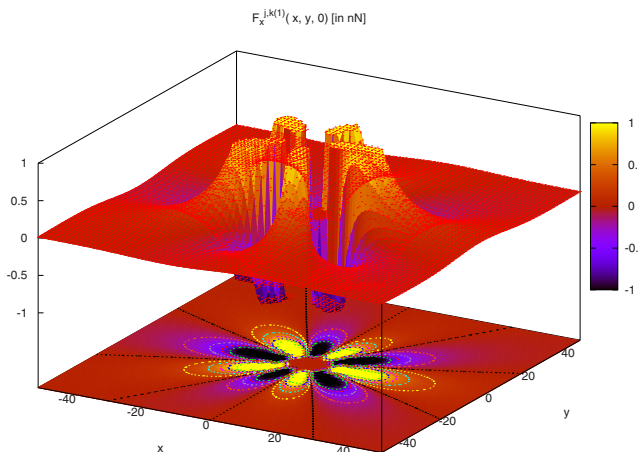
where

FIG. 5. (Color online) Part of spatial profile of $F_x^{j,k(2)}$ with values between −1 and 1 nN for the interaction between dipolar loops V_1 and V_1 having the same z-axis coordinate.

FIG. 4. (Color online) Part of spatial profile of $F_x^{j,k(1)}$ with values between −1 and 1 nN for the interaction between dipolar loops V_1 and V_2 having the same z-axis coordinate.
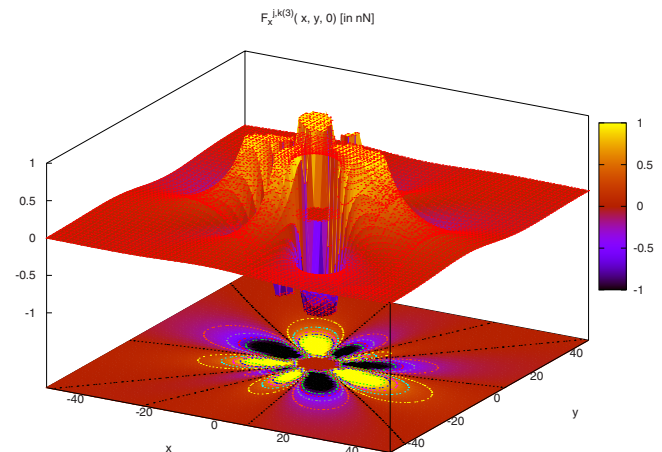

FIG. 6. (Color online) Part of spatial profile of $F_x^{j,k(3)}$ with values between −1 and 1 nN for the interaction between dipolar loops V_2 and V_2 having the same z-axis coordinate.
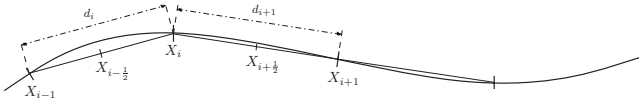
FIG. 7. Piecewise linear approximation of the dislocation curve, flowing finite volumes, and construction of dual volumes.

$$d_i = |\vec{X}_i - \vec{X}_{i-1}| = \sqrt{(X_i^x - X_{i-1}^x)^2 + (X_i^z - X_{i-1}^z)^2} \qquad (17)$$

are the distances between the nodes (we recall that Γ is located in the slip plane Σ, and therefore the y coordinate vanishes).

The values F_i are a piecewise constant approximation of the function F over the dual volume $\mathcal{V}_i$ with

$$F_i = F(\vec{X}_i).$$

Replacing the terms on the right-hand side of Eq. (16) by finite differences and by averaged values, respectively, the following system of ordinary differential equations (ODE's) is obtained (compare with Ref. 14)

$$B\frac{d\vec{X}_i}{dt} = \varepsilon \frac{2}{d_i + d_{i+1}} \left(\frac{\vec{X}_{i+1} - \vec{X}_i}{d_{i+1}} - \frac{\vec{X}_i - \vec{X}_{i-1}}{d_i} \right)$$
$$+ \frac{2}{d_i + d_{i+1}} F_i \frac{\vec{X}_{i+1}^\perp - \vec{X}_{i-1}^\perp}{2}, \quad i = 1, \ldots, M-1. \quad (18)$$

The initial conditions for this problem are given by the distribution of initial node positions given by values $s_1, \ldots, s_{M-1}$ of the arc-length parameter

$$\vec{X}_i(0) = \vec{X}_{ini}(s_i), \quad i = 1, \ldots, M-1.$$

The discretization of Γ also influences the stress contribution of the dislocation curve to the motion equation of the jth dipolar loop due to term [Eq. (12)]. The contributions of each curve segment are summed to obtain approximation of $F_x^{c,(j)}$ for which we use the same notation

$$F_x^{c,(j)}(t) = \sum_{i=0}^{M-1} \sigma_{xy}(X_{i+1/2}^x(t) - x^{(j)}(t), -y^{(j)}, X_{i+1/2}^z(t) - z^{(j)})$$
$$\times b_{curve}(X_{i+1}^z(t) - X_i^z(t)), \quad (19)$$

where $[x^{(j)}(t), y^{(j)}, z^{(j)}]$ is the center of the dipolar loop at time t, and $y^{(j)}$ and $z^{(j)}$ are fixed and time independent.

The driving term $F_{x,total}^{(j)}$ in Eq. (4) is then evaluated according to Eq. (11). Note that it depends on the nodal positions $\vec{X}_i(t), i = 0, \ldots, M$.

$$\frac{dx^{(j)}(t)}{dt} = \frac{1}{BP} F_{x,total}^{(j)}(\vec{X}_0(t), \ldots, \vec{X}_M(t), x^{(0)}(t), \ldots, x^{(N)}(t)),$$
$$j = 1, \ldots, N. \quad (20)$$

The discretized evolution problem is completed by initial and boundary conditions and has the following form:

$$B\frac{d\vec{X}_i}{dt} = \varepsilon \frac{2}{d_i + d_{i+1}} \left(\frac{\vec{X}_{i+1} - \vec{X}_i}{d_{i+1}} - \frac{\vec{X}_i - \vec{X}_{i-1}}{d_i} \right)$$
$$+ \frac{2}{d_i + d_{i+1}} F_i \frac{\vec{X}_{i+1}^\perp - \vec{X}_{i-1}^\perp}{2}, \quad i = 1, \ldots, M-1. \quad (21)$$

$$\frac{dx^{(j)}(t)}{dt} = \frac{1}{BP} F_{x,total}^{(j)}(\vec{X}_0(t), \ldots, \vec{X}_M(t), x^{(0)}(t), \ldots, x^{(N)}(t)),$$
$$j = 1, \ldots, N. \quad (22)$$

$$\vec{X}_0 = \vec{X}_{fixed,0}, \quad \vec{X}_M = \vec{X}_{fixed,L}, \quad (23)$$

$$\vec{X}_i(0) = \vec{X}_{ini}(s_i), \quad i = 1, \ldots, M-1, \quad x^{(j)}(0) = x_{ini}^{(j)},$$
$$j = 1, \ldots, N. \quad (24)$$

This problem is a system of ODE's depending on time. It is solved by the Runge–Kutta fourth-order scheme according to Ref. 24.

B. Redistribution of nodes along the dislocation curve

Dynamics of the interaction between the dislocation curve and the dipolar loops contains several time scales related to the motion of the dislocation, to the motion of the dipolar loops and to their mutual influence. For example, an imposed external periodically variable total strain causes a periodical motion of the dislocation (expansion and shrinking) with a relatively short time scale. This motion brings changes in the position of the dipolar loops with another, longer time scale. Frequently, the model must cover time intervals of order of magnitude larger to make corresponding physical behavior apparent. This requirement can become difficult to fulfill when using the discrete model [Eqs. (21)–(24)] without any additional improvement.

Such difficulties are shown in Fig. 8 where dynamics of a single dislocation curve and two dipolar loops is presented. The model setting is summarized in Table I. This computational study considers one dipolar loop (left) of the type V_2 and placed 5 nm above the slip plane of the dislocation curve. Another dipolar loop (right) of the type V_1 is placed 5 nm below the slip plane of the dislocation curve. The initial configuration for time $t=0$ is shown in Fig. 8(a). The inclination of the initially straight dislocation curve with respect to the Burgers vector is 30°. Position of the curve and loops is shown at four different time moments close to the time $t=36$ s in Fig. 8(b) (corresponds to more than 56 load cycles) and at four different time moments close to the time $t=56$ s in Fig. 8(d) (corresponds to more than 87 load cycles). An enlarged detail of Fig. 8(b) is in Fig. 8(c) from which a nonuniform distribution of discretization nodes along the dislocation curve can be observed. After a certain time, the numerical computation of this example becomes unstable—the discretization nodes shift away from each other along some parts of the dislocation curve. This is caused by the force interaction with the dipolar loops and by long time intervals covered by the simulation. These two effects overcome the natural redistribution property of Eq. (3). It is therefore necessary to derive an enhanced redistribution of the nodes along the dislocation curve (in the tangential direction) which would stabilize nodes during long-term computations.

The redistribution algorithms have been discussed, e.g., in Refs. 25–29 for closed curves where tangential motion of
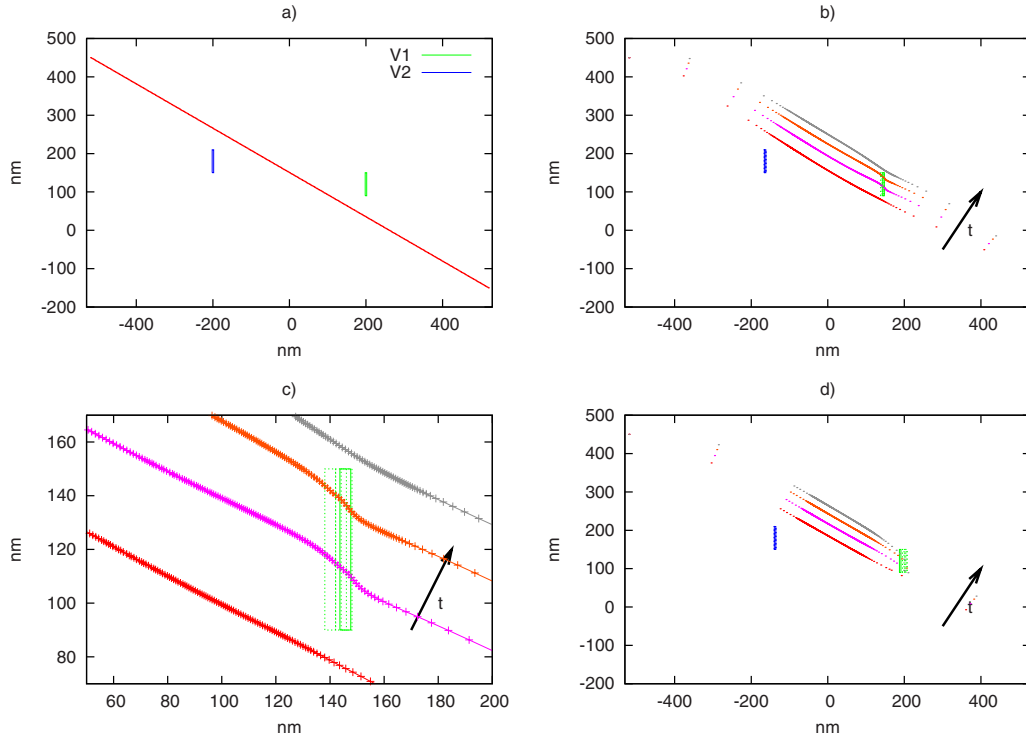
FIG. 8. (Color online) Interaction dynamics between a dislocation and two dipolar loops of V_1 and V_2 type computed without help of a tangential redistribution of nodes along the dislocation curve. Initial condition is shown in part (a). After 56 load cycles, i.e., close to $t=36$ s, part (b) shows mutual configuration of the dislocation and of the loops at four subsequent time moments differing by 0.05 s. Detail of this configuration is in part (c) from which nonuniform distribution of nodes along the dislocation can be observed. After 87 load cycles, i.e., close to $t=56$ s, part (d) shows mutual configuration of the dislocation and of the loops at four subsequent time moments differing by 0.05 s.

the nodes is not limited by the shape of the curve. Dislocation curves considered in this article are open. The tangential motion of points is then limited by the fixed ends. We therefore modify approaches available for closed curves and allow a tangential motion for the nodes inside the dislocation curve only.

For this purpose the governing Eq. (3) for the dislocation motion is modified by adding a term $\alpha \partial_s \vec{X}$ acting in the tangential direction which does not modify the curve motion

$$B \partial_t \vec{X} = \varepsilon \partial_{ss}^2 \vec{X} + F \partial_s \vec{X}^\perp + \alpha \partial_s \vec{X}, \qquad (25)$$

here α is the coefficient of the tangential motion which is specified below.

The tangential term is introduced into the discrete Eq. (21). Here instead of discretizing $\alpha \partial_s \vec{X}$ by

TABLE I. Table of parameters used in simulations.

Parameter	Notation	Value
Drag coefficient	B	5×10^{-5} s^{-1}
Line tension	ϵ	4 MPa m
Burgers vector	b	0.256 nm
Initial length of the dislocation curve	L_0	1200 nm
Density of dislocations	ρ	9.2×10^{12} m^{-2}
Amplitude of periodic external force term	ε_A	0.0017
Frequency of periodic external force term	f	1.57 s^{-1}
Shear modulus	μ	80 GPa

$$\alpha_i \frac{\vec{X}_{i+1} - \vec{X}_{i-1}}{d_i + d_{i+1}},$$

similarly to the force term in Eq. (21), another discretization is used

$$\alpha_i \frac{\vec{X}_{i+1} - \vec{X}_{i-1}}{|\vec{X}_{i+1} - \vec{X}_{i-1}|}.$$

The reason is that for higher curvature at the node $\vec{X}_i$, the distance $|\vec{X}_{i+1} - \vec{X}_{i-1}|$ fits better into the numerical approximation than the sum of distances d_i and d_{i+1}, as discussed in Refs. 28 and 30. The modified discrete evolution law then becomes

$$B \frac{d\vec{X}_i}{dt} = \varepsilon \frac{2}{d_i + d_{i+1}} \left(\frac{\vec{X}_{i+1} - \vec{X}_i}{d_{i+1}} - \frac{\vec{X}_i - \vec{X}_{i-1}}{d_i} \right)$$
$$+ \frac{2}{d_i + d_{i+1}} F_i \frac{\vec{X}_{i+1}^\perp - \vec{X}_{i-1}^\perp}{2} + \alpha_i \frac{\vec{X}_{i+1} - \vec{X}_{i-1}}{|\vec{X}_{i+1} - \vec{X}_{i-1}|},$$
$$i = 1, \ldots, M - 1. \qquad (26)$$

When specifying a suitable parameter α for an open curve with fixed ends, obvious conditions must be satisfied

$$\alpha_0(t) = \alpha_M(t) = 0, \quad \forall \, t \in (0, T).$$

A class of curvature-driven problems can be treated by the redistribution of the nodes based on the curvature as discussed in Refs. 25, 28, 30, and 31. In this case, the nodes accumulate along parts of the curve with higher curvature. In

case of dislocation dynamics, the dislocation is curved close to the dipolar loops whose position is not *a priori* known. Redistribution of the nodes to the proximity of the dipolar loops then can be delayed. Accuracy of simulations is also influenced by the approximation of the term [Eq. (8)] describing the plastic strain carried by a curve segment.

Derivation of a suitable form of α_i, $i = 1, \ldots, M-1$, then proceeds by means of a change of the arc-length parametrization to the fixed-domain parametrization of the curve Γ governed by the law [Eq. (1)] as it has been shown in Ref. 32. Assume that Γ is parametrized by the mapping $x = x(t, u)$ for $u \in [0, 1]$ being the fixed-domain parameter. We then define

$$g(u, t) = |\partial_u x(u, t)|.$$

Then there is a relation between the fixed-domain parametrization by u and the arc-length parametrization by s as follows:

$$\mathrm{d}s = g\,\mathrm{d}u. \tag{27}$$

Denote the right-hand side of Eq. (1) as $\beta = \varepsilon \kappa_\Gamma + F$ and express the quantity A by means of both parametrizations as

$$A = \frac{1}{L}\int_\Gamma \kappa_\Gamma \beta \mathrm{d}s = \frac{1}{L}\int_0^1 \kappa_\Gamma \beta g\,\mathrm{d}u. \tag{28}$$

If we set

$$\partial_s \alpha = \kappa_\Gamma \beta - A,$$

we have in terms of the fixed domain parametrization

$$\frac{1}{g}\partial_u \alpha = \kappa_\Gamma \beta - A. \tag{29}$$

We then obtain the simplest model preserving relative local lengths.

1. Relative-length preserving redistribution

Equation (29) can be rewritten into the form

$$\partial_u \alpha = \kappa_\Gamma \beta g - Ag,$$

from which we obtain a formula for α

$$\alpha(t, 0) = 0, \tag{30}$$

$$\alpha(t, u) = \int_0^u \kappa_\Gamma \beta g\,\mathrm{d}\xi - A\int_0^u g\,\mathrm{d}\xi. \tag{31}$$

Such a choice of α yields (see Ref. 32)

$$\frac{g(u, t)}{L(t)} = \frac{g(u, 0)}{L(0)} \quad \text{for any } u \in [0, 1], \quad t \in (0, T),$$

what in fact expresses the preservation of relative local lengths. Moreover, the requirement for $\alpha(t, 1)$ is easily fulfilled

$$\alpha(t, 1) = \int_0^1 \kappa_\Gamma \beta g\,\mathrm{d}\xi - A\int_0^1 g\,\mathrm{d}\xi = AL - AL = 0.$$

Conservation of the relative local lengths is a suitable property for the model of dislocation dynamics. We therefore convert Eq. (31) into the arc-length form

$$\alpha(t, s) = \int_0^s \kappa_\Gamma \beta \mathrm{d}\sigma - A\int_0^s \mathrm{d}\sigma. \tag{32}$$

Using discrete form of the differential transformation in Eq. (27)

$$g \approx \frac{|\vec{X}_{i+1} - \vec{X}_i|}{\Delta u}, \quad L(t) \approx \sum_{i=0}^{M-1} |\vec{X}_{i+1} - \vec{X}_i|,$$

the formula in Eq. (32) can be transformed into the discrete version

$$L_i(t) = \sum_{j=0}^i d_j,$$

$$\alpha_0(t) = 0, \tag{33}$$

$$\alpha_i(t) = \sum_{j=0}^i \kappa_{\Gamma,j}\beta_j d_j - \frac{L_i(t)}{L(t)}\sum_{j=0}^M \kappa_{\Gamma,j}\beta_j d_j, \tag{34}$$

where d_j is the distance of the neighboring nodes defined in Eq. (17). The quantities $\kappa_{\Gamma,j}$ and β_j are expressed in terms of the parametrization $\vec{X} = \vec{X}(t, s)$. The Frenet formula gives

$$\kappa_\Gamma \cdot \vec{N} = \partial_{ss}^2 \vec{X}, \tag{35}$$

where $\vec{N}$ denotes the normal vector

$$\vec{N} = \partial_s \vec{X}^\perp \approx \frac{(\vec{X}_{i+1} - \vec{X}_{i-1})^\perp}{|\vec{X}_{i+1} - \vec{X}_{i-1}|}.$$

Using the scalar product with $\vec{N}$ on both sides of the Frenet formula (35) we get

$$\kappa_\Gamma = \partial_{ss}^2 \vec{X} \cdot \vec{N}. \tag{36}$$

Discretizing this relationship [compared with Eq. (26)] we obtain

$$\kappa_{\Gamma,i} = \frac{2}{d_i + d_{i+1}}\left(\frac{\vec{X}_{i+1} - \vec{X}_i}{d_{i+1}} - \frac{\vec{X}_i - \vec{X}_{i-1}}{d_i}\right) \cdot \frac{(\vec{X}_{i+1} - \vec{X}_{i-1})^\perp}{|\vec{X}_{i+1} - \vec{X}_{i-1}|}. \tag{37}$$

The formula for β_i is obtained from Eq. (26) too.

$$\beta_i = \varepsilon \frac{2}{d_i + d_{i+1}}\left(\frac{\vec{X}_{i+1} - \vec{X}_i}{d_{i+1}} - \frac{\vec{X}_i - \vec{X}_{i-1}}{d_i}\right)$$
$$+ \frac{2}{d_i + d_{i+1}}F_i \frac{\vec{X}_{i+1}^\perp - \vec{X}_{i-1}^\perp}{2}. \tag{38}$$

In comparison to the analytical formulae (30) and (31) preserving relative local lengths, the discrete version [Eq. (34)] preserves them approximately only. As it can be seen from Fig. 9, numerical behavior is improved only slightly in com-
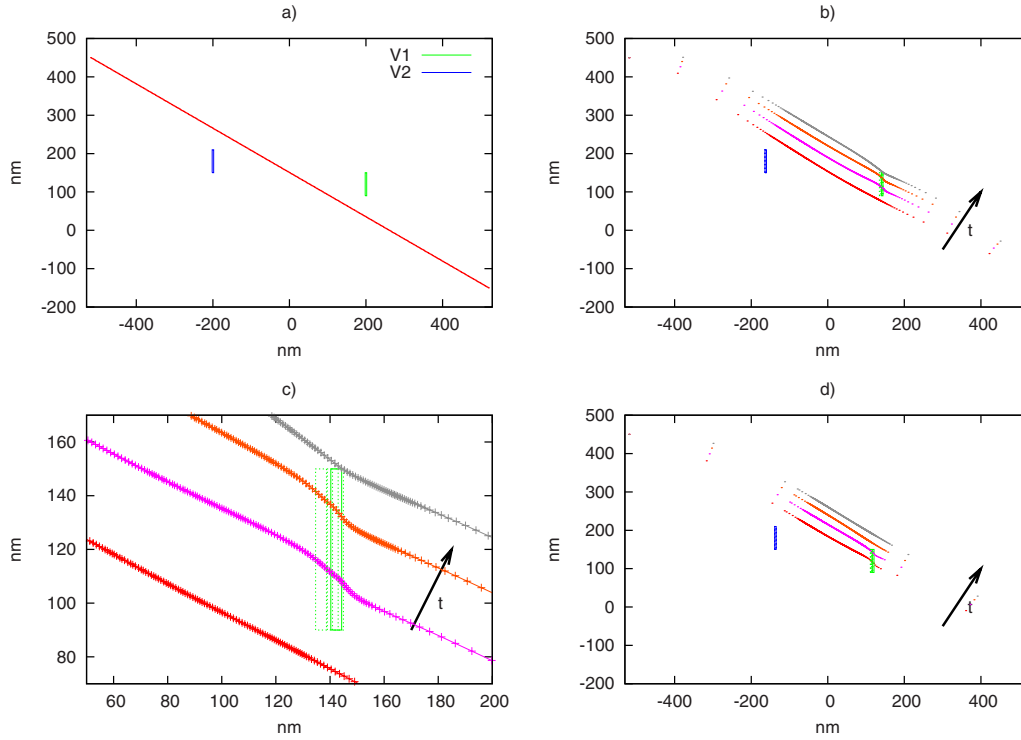
FIG. 9. (Color online) Interaction dynamics between a dislocation and two dipolar loops of V_1 and V_2 type is computed with help of the relative-length preserving redistribution. The setting and presentation of the result is identical to the simulation presented in Fig. 8. Time evolution is indicated by an arrow.

parison with Fig. 8. This is caused by the predominant nature of the interaction forces overcoming this type of redistribution.

2. Asymptotically uniform redistribution

A stronger type of redistribution is therefore needed. Let ω be a constant to be specified later. Let us use the quantity A defined in Eq. (28). The expression for α is

$$\frac{1}{g}\partial_u\alpha = \kappa_\Gamma\beta - A + \omega\left(\frac{L}{g} - 1\right),$$

from which we get

$$\partial_u\alpha = \kappa_\Gamma\beta g - Ag + \omega(L - g).$$

In the continuous case α is given by

$$\alpha(t,0) = 0,$$

$$\alpha(t,u) = \int_0^u \kappa_\Gamma\beta g\,d\xi - A\int_0^u g\,d\xi + \omega\left(L\int_0^u d\xi - \int_0^u g\,d\xi\right).$$

Similarly to the previously described *relative local length preserving* case, for $\alpha(t,1)$ it holds

$$\alpha(t,1) = \int_0^1 \kappa_\Gamma\beta g\,d\xi - A\int_0^1 g\,d\xi + \omega\left(L\int_0^1 d\xi - \int_0^1 g\,d\xi\right)$$

$$= AL - AL + \omega(L \cdot 1 - L) = 0.$$

The discrete formula for α_i in the case of asymptotically uniform redistribution of nodes reads as

$$L_i(t) = \sum_{j=0}^{i} d_j,$$

$$\alpha_0(t) = 0,$$

$$\alpha_i(t) = \sum_{j=0}^{i} \kappa_{\Gamma,j}\beta_j d_j - \frac{L_i(t)}{L(t)}\sum_{j=0}^{M} \kappa_{\Gamma,j}\beta_j d_j$$
$$+ \omega\left(\frac{L(t)}{d_i(M-1)} - 1\right). \tag{39}$$

Under the assumptions that $\omega > 0$ is constant (e.g., $\omega = 100$) we refer to Ref. 32 to state the behavior of the local length as t grows

$$\frac{g(u,t)}{L(t)} \to 1 \quad \text{as } t \to T_{\max}$$

uniformly with respect to $u \in [0,1]$.   (40)

Figure 10 shows that under identical setting as it was presented in Figs. 8 and 9, the nodes remain uniformly distributed along the dislocation in long-term computations.

IV. SIMULATION RESULTS AND DISCUSSION

Main goal of the article was to present a reliable simulation method which allows to perform computations for long time periods. In Sec. III it has been concluded that the method of the asymptotically uniform redistribution of nodes satisfies this requirement. As a further test, the method is employed in a preliminary study of a loop clustering considered to be one of elementary processes leading to a dipolar
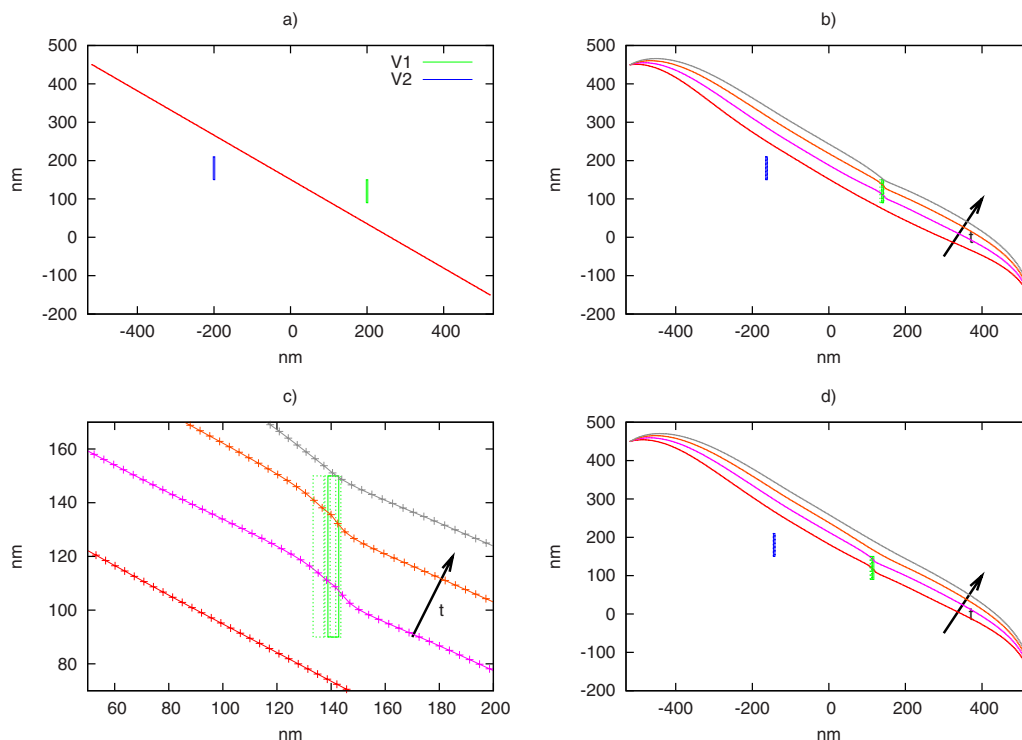
FIG. 10. (Color online) Interaction dynamics between a dislocation and two dipolar loops of V_1 and V_2 type computed with help of the asymptotically uniform redistribution. The setting and presentation of the result is identical to the simulation presented in Fig. 8. Time evolution is indicated by an arrow.

dislocation structure formation. Basic setup of the computations is the same as in Sec. III—see Table I. The dislocation is exposed to the local stress σ_{local} given by Eq. (9). In the imposed cyclic shear $\varepsilon_{tot}(t)$ with amplitude ε_A and frequency f from Table I, the dislocation oscillates in the environment of loops. In Fig. 11 there are several time levels of dynamics consisting of a single dislocation curve (initial length 1.2 μm, the mixed orientation of 30° with respect to the Burgers vector), five vacancy dipolar loops V_1 with y coordinate equal to -10, 10 (twice), 15, and 20 nm, and five vacancy dipolar loops V_2 with y coordinate equal to -10, 10 (twice), -15, and -20 nm. The left-hand side of the figure contains 3D plots with positions of the curve and loops, whereas the right-hand side contains two-dimensional (2D) projection of their positions onto the slip plane of the dislocation curve. In each record, four closely following time levels (differing of 0.05 s—8% of load cycle—each from other) are brought together in order to provide better understanding of dynamics at given time moments. For the result presented in Fig. 11, mutual interactions between dipolar loops captured by the model are essential.

The simulation has been performed in order to study the clustering phenomenon which occurs rather abruptly. It is first observed at $t=46$ s—after 72 load cycles. In the following time levels, the cluster does not substantially change its shape.

In general, the cluster formation highly depends on the initial conditions where the initial positions of the dipolar loops play important role. Moreover, the clustering is not a rule. A change in types of dipolar loops (using the same initial positions) produces different results and does not necessarily lead to clustering. This fact is illustrated in Fig. 12.

Four different initial setups of vacancy dipolar loop configurations were used for the simulations. Here, five dipolar loops of type V_1 and five dipolar loops of type V_2 were used with positive or negative y coordinate ranging between 10 and 20 nm. The left-hand side graphs show the initial setups ($t=0$ s), while the right-hand side graphs show the simulation results close to the time $t=166$ s—after 260 load cycles. In Figs. 12(a) and 12(c), there is no apparent clustering. In Fig. 12(b) clustering occurs. In Fig. 12(d), two smaller clusters seem to be formed. Clear correlation between occurrence of clustering and composition of the loop set has not yet been detected.

The above presented results represent a test of the proposed computational method in case of larger number of loops. A further systematic study of a loop clustering would be needed. From a broader viewpoint, the loop clustering is one of several mechanisms of dipolar structure pattering. One could also consider interaction among glide dislocations, loop and dislocation generation, and annihilation subjected to laws of continuum crystal mechanics (stress equilibrium and compatibility).

The pattering phenomenon has also been studied by other approaches. The model of discrete dislocation dynamics considering segments of the dislocation curves moving over a discrete lattice was used for simulations of activity of a large number of dislocations in a volume element of the size ~ 10 μm with periodic boundary conditions and with a realistic dislocation density. As it can be seen from Refs. 33–35, it already reached some traces of initial pattering. On the other hand, the models of discrete dislocation dynamics based on parametric methods, which discretize dislocation curves into piecewise linear (the model presented here) or
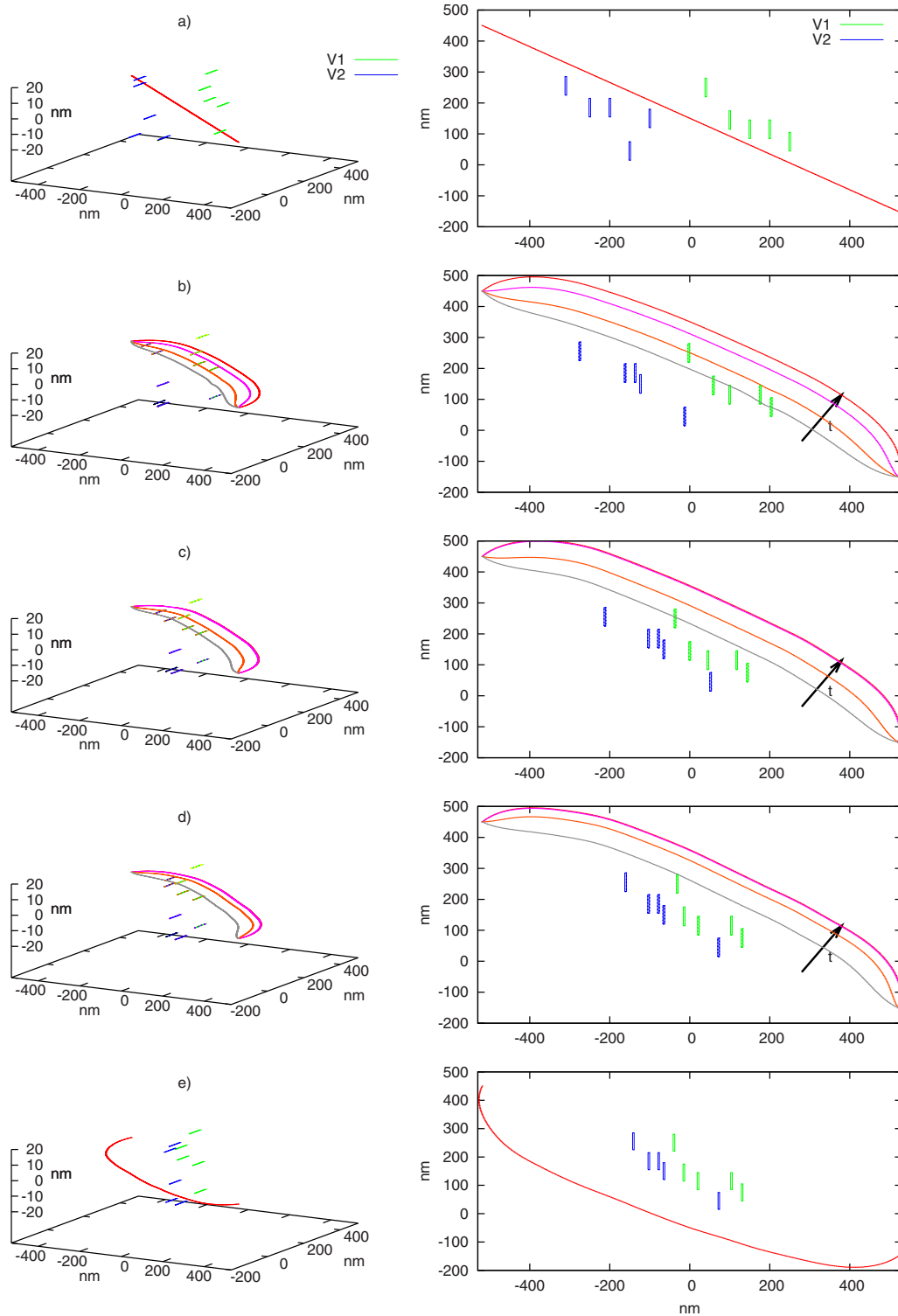
FIG. 11. (Color online) Interaction dynamics between a dislocation and ten dipolar loops of of V_1 and V_2 type. Graphs on left show spatial positions of interacting objects, graphs on right show projection of the positions onto the slip plane. The initial configuration is in part (a), the configuration after 72 load cycles, i.e., close to $t=46$ s in part (b), the configuration after 178 load cycles, i.e., close to $t=114$ s in part (c), the configuration after 260 load cycles, i.e., close to $t=166$ s in part (d), and the configuration after 312 load cycles, i.e., close to $t=199$ s in part (e). Parts (b)–(e) show mutual configuration of the dislocation and of the loops at four subsequent time moments differing by 0.05 s with time evolution indicated by an arrow.

into piecewise polynomially represented segments, may require more computational capacity. On the other hand, the parametric methods are more accurate in capturing details of the dislocation and loops interactions. As our preliminary results indicate, the clustering is sensitive to these details. This opens a further perspective for the described approach.

As dislocation pattering is a result of a collective behavior of a large number of dislocations and loops a continuous description is a useful tool. A statistical derivation of continuous distribution of dislocations from discrete dislocation dynamics has been suggested by Groma *et al.*[36–40] The idea was to study a simplified model of straight parallel edge
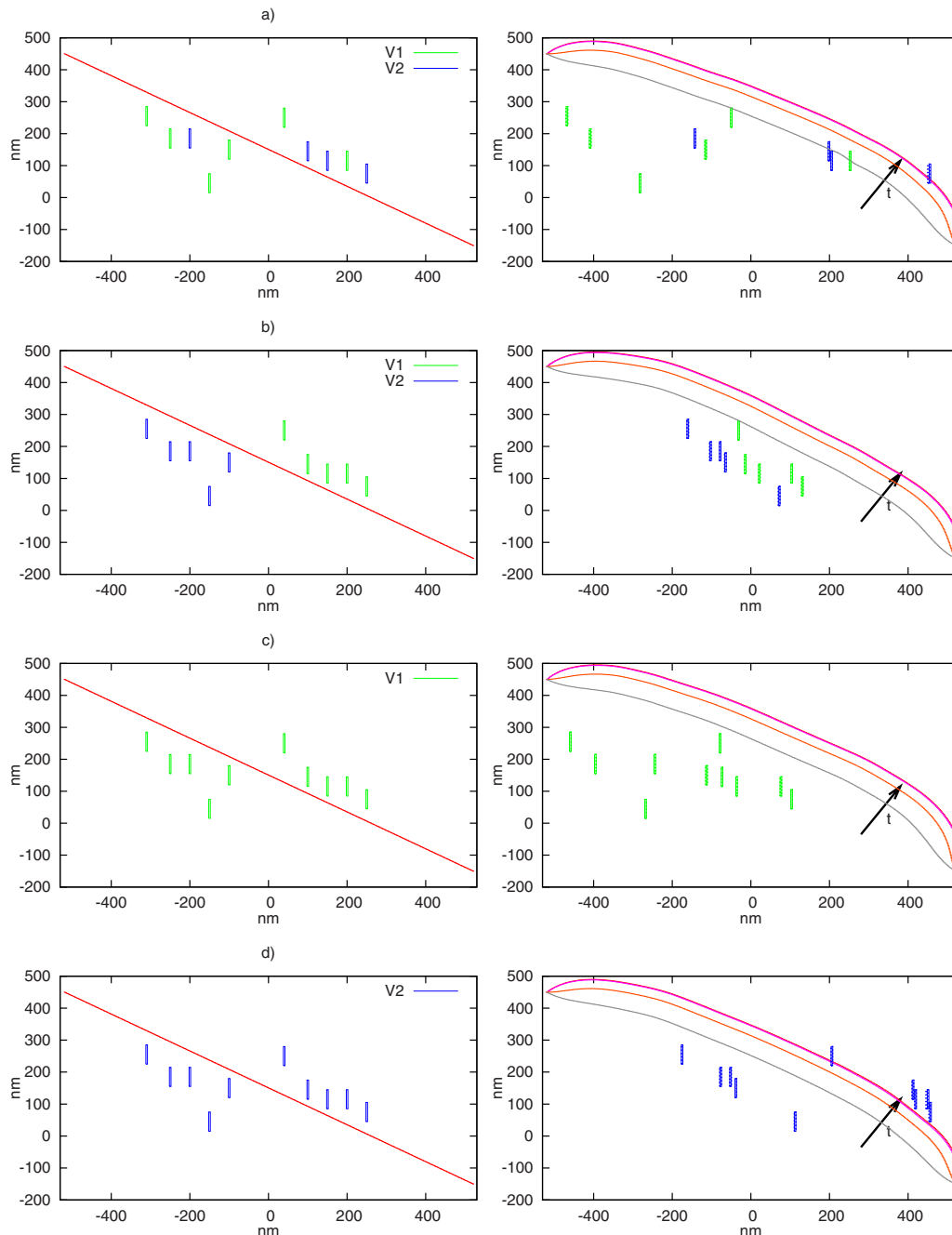
FIG. 12. (Color online) Interaction dynamics between a dislocation and ten dipolar loops of of V_1 and V_2 type with four different initial configurations. After 260 load cycles, i.e., close to $t=166$ s, each of graphs on right shows mutual configuration of the dislocation and of the loops at four subsequent time moments differing by 0.05 s with time evolution indicated by an arrow.

dislocations of a single slip system represented by points of intersection of the dislocation lines with the plane of deformation. Thus, the problem was reduced to statistics of point objects, where the tools of standard statistical mechanics were employed. This idealized model revealed one of the main problems of this approach: an adequate description of the short range correlations among dislocations. In the derived averaged continuum model, the correlations result in nonlocal effects which play a decisive role in modeling of dislocation pattering and size effects. In 2D idealized models, there have been partly successful attempts[38,39] to determine the correlation functions by means of a statistical evaluation of massive dynamics simulations of discrete straight edge dislocations. The statistical approach mentioned above has been applied to curved glide dislocations and dipolar dislocation loops in Ref. 41. The resulting continuous constitutive equations are expressed through correlation functionals. Their determination would require a careful description of interactions in the close vicinity of a dislocation or a loop. The method proposed and tested in this article could provide the data on local arrangement in loop clustering caused by a moving dislocation.

ACKNOWLEDGMENTS

[1] T. Mura, *Micromechanics of Defects in Solids* (Kluwer Academic, Netherlands, 1987).
[2] J. P. Hirth and J. Lothe, *Theory of Dislocations* (Wiley, New York, 1982).
[3] J. Kratochvíl and M. Saxlová, Phys. Scr. **T49B**, 399 (1993).
[4] F. Kroupa, Phys. Status Solidi **9**, 27 (1965).
[5] J. Kratochvíl, F. Kroupa, and L. P. Kubin, *Deformation-Induced Microstructures: Analysis and Relation to Properties*, Proceedings of the 20th Risoe International Symposium on Material Science (Risoe National Laboratory, Roskilde, 1999), pp. 387–392.
[6] M. Saxlová, J. Kratochvíl, and J. Zatloukal, Mater. Sci. Eng., A **234–236**, 205 (1997).
[7] J. Kratochvíl, Mater. Sci. Eng., A **309–310**, 331 (2001).
[8] B. Devincre and L. P. Kubin, Mater. Sci. Eng., A **8–14**, 234 (1997).
[9] M. C. Fivel and G. R. Canova, Modell. Simul. Mater. Sci. Eng. **7**, 753 (1999).
[10] M. Rhee, H. M. Zbib, J. P. Hirth, H. Huang, and T. de la Rubia, Modell. Simul. Mater. Sci. Eng. **6**, 467 (1998).
[11] M. Tang, L. P. Kubin, and G. R. Canova, Acta Mater. **46**, 3221 (1998).
[12] N. M. Ghoniem and L. Z. Sun, Phys. Rev. B **60**, 128 (1999).
[13] N. M. Ghoniem, J. Huang, and Z. Wang, Philos. Mag. Lett. **82**, 55 (2002).
[14] V. Minárik, J. Kratochvíl, K. Mikula, and M. Beneš, *Numerical Simulation of Dislocation Dynamics*, Numerical Mathematics and Advanced Applications, ENUMATH 2003 (Peer Reviewed Proceedings) edited by M. Feistauer, V. Dolejší, P. Knobloch, and K. Najzar (Springer-Verlag, Berlin, 2004), pp. 631–641.
[15] V. Minárik, J. Kratochvíl, and K. Mikula, *Numerical Simulation of Dislocation Dynamics by Means of Parametric Approach*, Proceedings of the Czech Japanese Seminar in Applied Mathematics, M. Beneš, J. Mikyška, and T. Oberhuber (Czech Technical University in Prague, Prague, 2005), pp. 128–138.
[16] J. Huang, N. M. Ghoniem, and J. Kratochvíl, Modell. Simul. Mater. Sci. Eng. **12**, 917 (2004).
[17] M. Beneš, Acta Math. Univ. Comen. **70**, 123 (2001).
[18] K. Deckelnick, G. Dziuk, and C. M. Elliott, Acta Numerica **14**, 139 (2005).
[19] G. deWit and J. S. Koehler, Phys. Rev. **116**, 1113 (1959).
[20] R. Sedláček, Philos. Mag. Lett. **76**, 275 (1997).
[21] J. Křišťan and J. Kratochvíl, Philos. Mag. **87**, 4593 (2007).
[22] Š. Verecký, J. Kratochvíl, and F. Kroupa, Phys. Status Solidi A **191**, 418 (2002).
[23] V. Minárik and J. Kratochvíl, Kybernetika **43**, 841 (2007).
[24] W. E. Schiesser, *The Numerical Method of Lines* (Academic, New York, 1991).
[25] T. Y. Hou, J. S. Lowengrub, and M. J. Shelley, J. Comput. Phys. **114**, 312 (1994).
[26] T. Y. Hou, I. Klapper, and H. Si, J. Comput. Phys. **143**, 628 (1998).
[27] D. Ševčovič and K. Mikula, SIAM J. Appl. Math. **61**, 1473 (2001).
[28] K. Mikula and D. Ševčovič, Math. Methods Appl. Sci. **27**, 1545 (2004).
[29] M. Kimura, Appl. Math. Lett. **7**, 69 (1994).
[30] K. Mikula and D. Ševčovič, Comput. Visualization Sci. **6**, 211 (2004).
[31] S. Yazaki, Kybernetika **43**, 913 (2007).
[32] D. Ševčovič, *Topics on Partial Differential Equations*, Jindřich Nečas Center for Mathematical Modeling, Lecture Notes (2008), Vol. 2, pp. 55–120.
[33] R. Madec, B. Devincre, and L. P. Kubin, Scr. Mater. **47**, 689 (2002).
[34] B. Devincre, L. P. Kubin, and T. Hoc, Scr. Mater. **57**, 905 (2007).
[35] B. Devincre, T. Hoc, and L. Kubin, Science **320**, 1745 (2008).
[36] I. Groma, Phys. Rev. B **56**, 5807 (1997).
[37] I. Groma and P. Balogh, Acta Mater. **47**, 3647 (1999).
[38] M. Zaiser, Phys. Rev. B **64**, 224102 (2001).
[39] I. Groma, F. F. Csikor, and M. Zaiser, Acta Mater. **51**, 1271 (2003).
[40] S. Yefimov, E. van der Giessen, and I. Groma, Modell. Simul. Mater. Sci. Eng. **12**, 1069 (2004).
[41] J. Kratochvíl and R. Sedláček, Phys. Rev. B **77**, 134102 (2008).